ADVANCED FUNCTIONAL MATERIALS

FULL PAPER

DOI: 10.1002/adfm.200701467

Topotactic Transformation of Single-Crystalline Precursor Discs into Disc-Like Bi_2S_3 Nanorod Networks**

By *Lianshan Li, Nijuan Sun, Youyuan Huang, Yao Qin, Nana Zhao, Jining Gao, Meixian Li, Henghui Zhou,* and *Limin Qi**

Hierarchical, two-dimensional (2D), disc-like networks consisting of crossed single-crystalline Bi_2S_3 nanorods have been synthesized via a novel 2D-template-engaged topotactic transformation process, which involves the formation of intermediate BiOCl single-crystalline discs and their subsequent chemical transformation into disc-like Bi_2S_3 nanofabrics. The transformation process from (001)-oriented BiOCl discs to disc-like Bi_2S_3 nanorod networks has been followed by using scanning electron microscopy (SEM), transmission electron microscopy (TEM), electron diffraction (ED) and X-ray diffraction (XRD), which revealed that the close matching between the lattice constants of the *c*-axis for orthorhombic Bi_2S_3 and the *a*- or *b*-axis for tetragonal BiOCl could be responsible for the preferential growth of [001]-oriented Bi_2S_3 nanorods on the top faces of (001)-oriented BiOCl discs along the two perpendicular [100] and [010] directions of BiOCl. The diameter of the Bi_2S_3 nanorods involved in the networks can be adjusted by changing the bismuth ion concentration in the reaction solution; moreover, an increase of the HCl concentration would prevent the formation of precursor BiOCl discs, leading to the formation of Bi_2S_3 nanostructures with varied morphologies. Charge–discharge curves and cyclic voltammograms of the obtained Bi_2S_3 nanostructures were measured to investigate their electrochemical hydrogen storage behaviors. It was found that the disc-like Bi_2S_3 nanorod networks could electrochemically charge and discharge with a capacity of 162 mA h g^{-1} at room temperature, indicating their potential applications in hydrogen storage, high-energy batteries, and catalytic fields.

1. Introduction

One-dimensional (1D) nanoscale building blocks, such as nanotubes, nanowires, nanorods, and nanobelts, have attracted intensive interest due to their importance in fundamental research and potential wide-ranging applications.[1] The controlled synthesis of 1D nanostructures and guiding them to ordered superstructures or complex functional architectures would offer great opportunities to explore their novel properties and to fabricate useful nanodevices.[2] In this regard, ordered nanoarrays have been obtained by the self-assembly of preformed uniform nanorods[3] and the template-directed growth of ordered nanowire arrays.[4] Moreover, the self-organized crystal growth of hierarchical architectures made of nanorods/nanowires has been successfully achieved without templates; notable examples include the chemical vapor deposition of ZnO nanobridges,[5a] nanocombs,[5b] nanopropeller arrays,[5c] and PbS hyperbranched nanowire networks,[5d] as well as the solution synthesis of multiarmed,[2a,6] multiple cone-shaped,[7] penniform,[8] snowflake-like,[9] and mesh-like[10] nanostructures. However, it remains a great challenge to develop rational synthetic methods to fabricate complex nanorod/nanowire superstructures with desired architectures.

In recent years, a variety of inorganic nanowires have been used as 1D precursor templates to generate novel 1D nanostructures through chemical transformation. Specifically, a variety of carbide nanowires were prepared by reacting carbon nanotubes with vapors of metal oxides or metal halides[11] while MgB_2 nanowires were obtained by reacting B nanowires with Mg vapor.[12] Notably, monocrystalline GaN nanotubes were successfully prepared via ''epitaxial casting'' by employing hexagonal ZnO nanowires as sacrificial templates for epitaxial overgrowth of thin GaN sheaths.[13] Meanwhile, solution-phase reaction has also been employed for the conversion of 1D sacrificial templates into 1D nanostructures. For example, $LiMo_3Se_3$ nanowires were used as a chemical template to prepare polycrystalline metal nanowires through redox reactions with metal salts in aqueous solutions.[14] Moreover, single-crystalline nanowires were successfully fabricated by topotactic transformation from single-crystalline 1D nanostructures; examples include the chemical transformation of Se nanowires into Ag_2Se nanowires[15] and the reversible transformation between CdSe nanorods and Ag_2Se nanorods via cationic exchange reactions.[16] However, such

[*] Prof. L. Qi, L. Li, N. Sun, Y. Huang, Y. Qin, N. Zhao, Dr. J. Gao, Prof. M. Li, Prof. H. Zhou
Beijing National Laboratory for Molecular Sciences (BNLMS)
State Key Laboratory for Structural Chemistry of Unstable and Stable Species
College of Chemistry, Peking University
Beijing 100871 (P.R. China)
E-mail: liminqi@pku.edu.cn

[**] This work was supported by MOST (2007CB936201), NSFC (20673007, 20325312, and 50521201) and SRFDP (20070001018).

ADVANCED FUNCTIONAL MATERIALS

template-engaged topotactic reactions were generally limited to the fabrication of individual nanorods/nanowires and it would be highly desirable to extend this strategy to directly fabricate hierarchical assemblies of 1D nanostructures with specific two-dimensional (2D) and three-dimensional (3D) architectures.

As a well-known layer-structured semiconductor with a direct band gap of 1.3 eV, bismuth sulfide (Bi_2S_3) has many potential applications including photovoltaics,[17] thermoelectrics,[18] X-ray computed tomography,[19] and electrochemical hydrogen storage.[20] Recently, considerable efforts have been devoted to the controlled synthesis of 1D Bi_2S_3 nanostructures as well as their ordered arrays or complex assemblies. Simple 1D Bi_2S_3 nanostructures such as nanorods, nanowires, and nanoribbons have been produced by various synthetic routes, such as solvothermal or hydrothermal process,[21] reflux reaction in an organic solvent,[22] and solventless thermolysis.[23] Bi_2S_3 nanowire arrays have been fabricated by a hydrothermal method[24] and by using anodic alumina membranes[25] or self-assembled monolayers[18,26] as templates. Moreover, some complex assemblies of Bi_2S_3 nanorods/nanowires including snowflake-like,[9] flower-like[20,27,28] and sheaflike[29] nanostructures have been obtained with the assistance of ionic liquids,[27] polymers,[28] biomolecules[9,20] or via a reaction in a hot organic solvent.[29] Interestingly, unusual 2D Bi_2S_3 nanofabrics consisting of crossed nanowires were obtained via solventless thermolysis at 225 °C in the presence of capping ligands; however, the yield was very low (<1%).[23] It is still challenging to explore the facile, high-yield synthetic routes to such superstructures of Bi_2S_3 nanorods/nanowires.

In this paper, a novel 2D-template-engaged topotactic reaction method was used to synthesize hierarchical disc-like Bi_2S_3 networks composed of perpendicularly aligned single-crystalline nanorods. It was revealed that these superstructures were formed by the preferential growth of [001]-oriented Bi_2S_3 nanorods on the top faces of (001)-oriented BiOCl discs along the two perpendicular [100] and [010] directions of BiOCl. To the best of our knowledge, this work represents the first topotactic transformation process capable of generating 2D networks consisting of single-crystalline nanorods. Moreover, the obtained Bi_2S_3 nanorod networks exhibited a good electrochemical hydrogen storage behavior with a capacity of 162 mA h g^{-1} at room temperature, indicating their potential applications in hydrogen storage, high-energy batteries, and catalytic fields.

2. Results and Discussion

2.1. Characterization of Bi2S3 Nanorod Networks

The synthesis of Bi_2S_3 nanorod networks were simply achieved by adding thioacetamide (TAA) to the hydrolysis solution of $BiCl_3$, which was followed by incubation at 60 °C for 60 hours. Figure 1 presents typical scanning electron microscopy (SEM) and transmission electron microscopy (TEM) images of the Bi_2S_3 networks obtained from a solution containing 2.25 mM $BiCl_3$ and 70 mM HCl. The low-magnification SEM image presented in Figure 1a shows that the predominant product is micrometer-sized discs with an average diameter about 2 μm (yield > 90%). An enlarged image is shown in Figure 1b, which suggests that the discs are actually circular nanofabrics consisting of one layer of interwoven nanorods and the thickness of the disc-like nanorod network is generally less than 50 nm. A representative TEM image of the nanofabric disc (Fig. 1c) confirms that the 2D network is made of crossed nanorods. An enlarged TEM image is shown in Figure ld, which reveals that the nanorods constituting the nanofabrics are rather uniform with a diameter about 30 nm and ranging in length from 150 to 200 nm. The X-ray diffraction (XRD) pattern of the disc-like nanorod networks is given in Figure 2, which shows that the nanofabrics are pure Bi_2S_3 crystals of the orthorhombic structure (Joint Committee on Powder Diffraction Standards (JCPDS) Card 17-0320: $a = 11.14$ Å, $b = 11.30$ Å, and $c = 3.981$ Å). It is worth noting that such an architecture of disc-like nanorod networks is unprecedented although 2D tin oxide nanomeshes[10] and bismuth sulfide nanofabrics,[23] which adopted irregular-plate-like morphologies, have been reported previously.

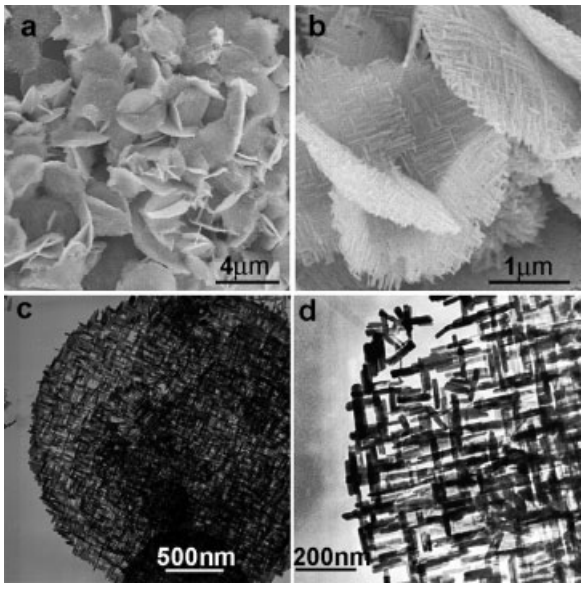

Figure 1. SEM (a, b) and TEM (c, d) images of disc-like Bi_2S_3 nanorod networks.

The crystalline structure of the individual Bi_2S_3 nanorods in the interwoven networks was characterized by the electron diffraction (ED) and high-resolution TEM (HRTEM) investigation. The ED pattern corresponding to the whole disc-like nanorod network shown in Figure 3a is presented in Figure 3b, which exhibits orderly arranged spots with a tetragonal symmetry, indicating that the perpendicularly aligned nanorods have high crystallinity and preferential growth direction. Basically, the diffraction spots consist of two identical

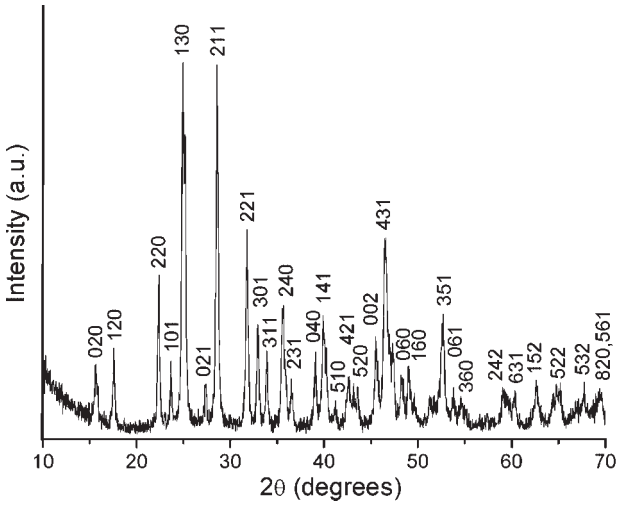

Figure 2. XRD pattern of disc-like Bi_2S_3 nanorod networks.

overlapping sets of patterns oriented at exactly 90° with respect to one another, which suggests that the crossed nanorods adopt a common growth direction. For simplicity, only one set of diffraction patterns corresponding to the parallel nanorods aligned along one direction are indexed to the $[1\bar{2}0]$ and $[1\bar{3}0]$ zone axes in Figure 3b. The elongation of the nanorods along the [001] direction is revealed by the four strong spots tetragonally arranged, which have a *d* spacing of 1.99 Å, corresponding to the (002) planes of the orthorhombic Bi_2S_3. Clear Moiré fringes can be observed from the high-magnification image of a crossed nanorod junction (Fig. 3c), revealing that the two crossed nanorods do not exhibit the same crystallographic orientation,[23] which is consistent with the fact that the nanorods in the fabric are all elongated along the [001] direction. A typical HRTEM image of an individual nanorod (Fig. 3d) exhibits clear lattice fringes corresponding to the (001) and (210) planes with the (001) plane perpendicular to the elongation direction of the nanorod, confirming that each nanorod is a single-crystalline nanorod elongated along the [001] direction. Moreover, additional HRTEM data obtained from different area of the network show that the lattice fringes parallel to the nanorod axis may be ascribed to planes other than the (210) plane, such as the (310) plane, while the lattice fringes perpendicular to the nanorod axis always exhibit the *d* spacing corresponding to the (001) plane. This result suggests that while all the [001]-oriented nanorods are parallel to the disc plane, they do not necessarily adopt a fixed orientation with respect to the disc plane, which is in agreement with the ED pattern that exhibits a set of diffraction patterns rather than a single diffraction pattern.

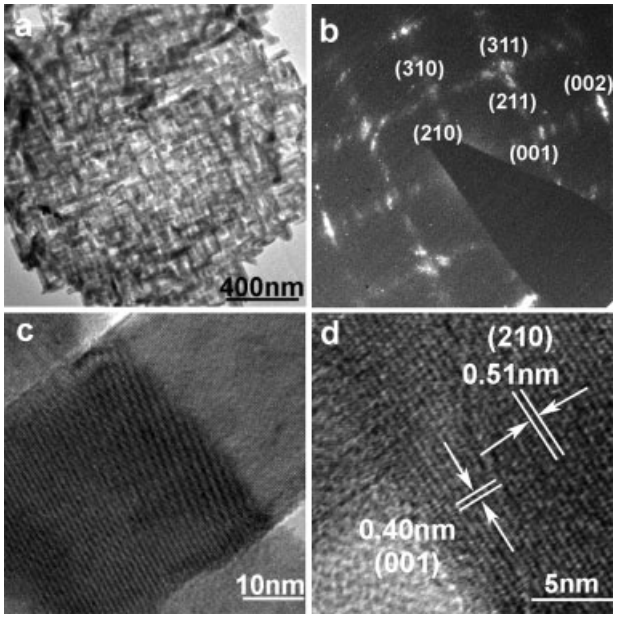

Figure 3. a) TEM image of a disc-like Bi_2S_3 nanorod network and b) the related ED pattern. c) High-magnification TEM image of Bi_2S_3 nanorod network showing clear Moiré fringes in the crossed nanorod junction. d) HRTEM image of Bi_2S_3 nanorods showing the (001) and (210) lattice fringes.

2.2. Formation Process of Bi_2S_3 Nanorod Networks

The formation process of the unique disc-like Bi_2S_3 nanorod networks was followed by examining the morphology and structure of the products obtained at different intervals of reaction time. Before the addition of TAA, a white precipitate formed in the hydrolysis solution of $BiCl_3$ upon the dilution of 3 M $BiCl_3$ solution with water. This solid precursor was collected after 2 h of aging in the hydrolysis solution without TAA. As shown in Figure 4a, the precursor exhibits micrometer-sized discs with smooth surfaces and a thickness about 20–50 nm. The corresponding XRD pattern shown in Figure 5 suggests that the precursor is pure BiOCl crystal with the tetragonal structure (JCPDS Card 82-0485: $a = 3.888$ Å and $c = 7.357$ Å). Moreover, the considerably intensified (001) reflection indicates that the discs could be single-crystalline discs with the top face of the (001) plane. The TEM image of the BiOCl discs (Fig. 4b) shows some ripple-like contrast that may be due to the stain resulting from the bending of the thin discs. The ED pattern corresponding to a single disc (Fig. 4c) exhibits sharp spots indexed to the [001] zone axis of the tetragonal BiOCl, confirming that each disc is a BiOCl single crystal with the top surface of the (001) plane. When TAA was added to the hydrolysis solution containing the BiOCl precursor, a transformation from the BiOCl discs to disc-like Bi_2S_3 nanorod networks occurred gradually, which was demonstrated by the XRD patterns shown in Figure 5. After 4 h of reaction, some diffraction peaks due to Bi_2S_3 appeared, indicating a partial transformation into Bi_2S_3. It can be seen from Figure 4d and e that the original solid discs evolved into disc-like nanorod networks. The ED pattern corresponding to a large area of the disc-like nanofabric exhibited many diffraction spots due to orthorhombic Bi_2S_3 in addition to the spots coming from tetragonal BiOCl. It is noteworthy that

ADVANCED FUNCTIONAL MATERIALS

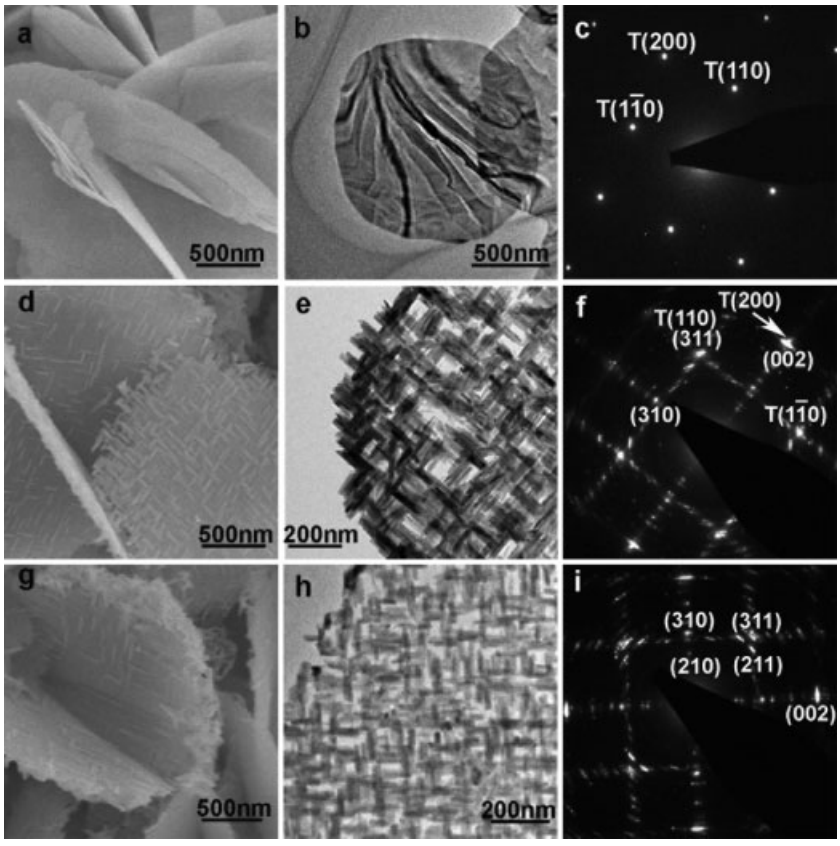

Figure 4. SEM (a, d, g) images, TEM (b, e, h) images, and ED patterns (c, f, i) of the BiOCl precursor discs (a–c) and the disc-like products obtained after reacting the BiOCl precursor with TAA for 4 h (d–f) and 10 h (g–i). The ED patterns were indexed based on tetragonal BiOCl and orthorhombic Bi_2S_3 with the spots attributed to tetragonal BiOCl denoted as "T" before the indices.

the tetragonally-symmetric Bi_2S_3 (002) spots ($d = 1.99$ Å) almost overlap the tetragonally-symmetric BiOCl (200) spots ($d = 1.94$ Å), strongly indicating an epitaxial registry between the BiOCl precursor disc and the Bi_2S_3 nanorod network. It may be inferred that the [001]-oriented Bi_2S_3 single-crystalline nanorods developed preferentially from the (001)-oriented BiOCl single-crystalline discs along the two perpendicular, equivalent [100] and [010] directions within the BiOCl disc plane, leading to the formation of the disc-like networks made of crossed Bi_2S_3 nanorods. When the reaction time was increased to 10 h, the apparent morphology of the product did not change considerably (Fig. 4g and h) but the diffraction spots due to BiOCl almost disappeared in the related ED pattern (Fig. 4i), indicating further conversion from BiOCl to Bi_2S_3. However, the XRD result shows that some peaks due to BiOCl are still evident at a reaction time of 10 h and a few weak peaks due to BiOCl can also be observed when the reaction time was prolonged to 44 h (Fig. 5), which suggests the transformation is still not complete. A further prolongation of the reaction time to 60 h would result in the formation of pure disc-like Bi_2S_3 nanorod networks shown in Figure 1, as revealed by the XRD pattern shown in Figure 2.

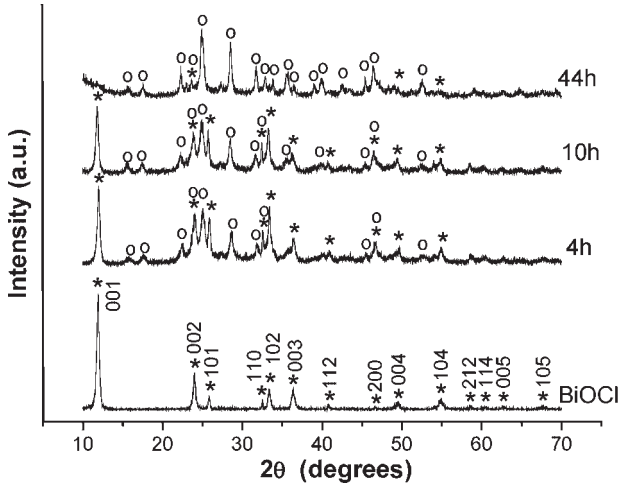

Figure 5. XRD patterns of the BiOCl precursor and the products obtained after reacting the BiOCl precursor with TAA for different times. The diffraction peaks due to BiOCl and Bi_2S_3 are denoted as "*" and "○", respectively.

The transformation from the original single-crystalline BiOCl discs to the final disc-like networks consisting of crossed single-crystalline Bi_2S_3 nanorods indicates a template-engaged topotactic reaction process, which was previously proposed for the topotactic transformation from single-crystalline Se nanowires to single-crystalline α-Ag_2Se nanowires due to the crystal lattice matching.[15] It is known that Bi_2S_3 nanocrystals have a strong tendency to grow along its *c*-axis into 1D nanostructures because the layer-structured Bi_2S_3 is composed of Bi_2S_3 bands elongating along the *c*-axis, which are kept together through van der Waals interactions.[30] In the current synthesis of disc-like Bi_2S_3 nanorod networks, the structural relationship between the *c*-axis of orthorhombic Bi_2S_3 ($c = 3.98$ Å) and the *a*- or *b*-axis of tetragonal BiOCl ($a = b = 3.89$ Å) could be responsible for the topotactic transformation from a single-crystalline disc-like template to a disc-like nanorod networks (Fig. 6). When the sulfur ions released from TAA diffused to the top surfaces of BiOCl single-crystalline discs with the top faces of the (001) plane, the sulfur ions might replace the oxygen ions and chlorine ions to generate [001]-oriented Bi_2S_3 single-crystalline nanorods lying on the top surfaces due to the lower solubility of Bi_2S_3. Moreover, these [001]-oriented Bi_2S_3 single-crystalline nanorods would tend to oriented along the two perpendicular [100] and [010] directions of BiOCl due to the close lattice matching between the *c*-axis of Bi_2S_3 and the *a*- or *b*-axis of BiOCl, leading to the formation of a layer of disc-like network consisting of crossed nanorods on the top faces of BiOCl discs. The close lattice matching indicates a

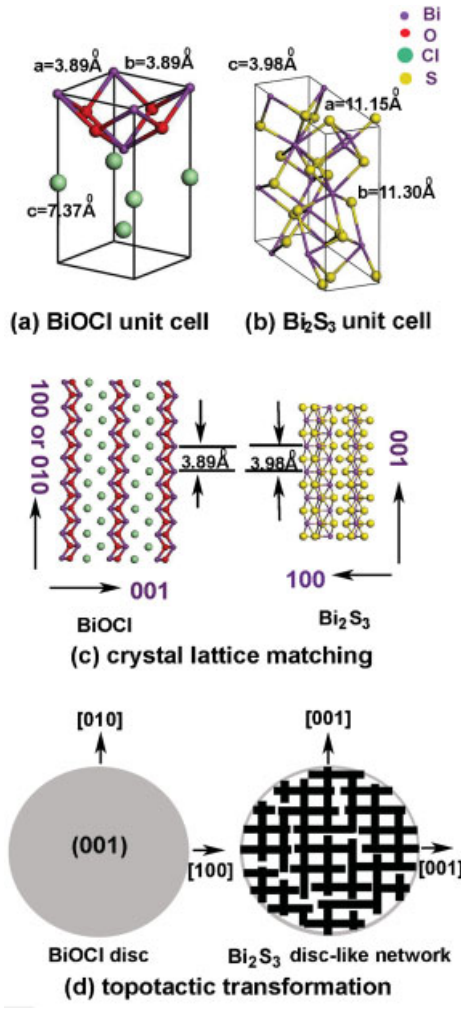

Figure 6. Schematic illustration of a) tetragonal BiOCl unit cell, b) orthorhombic Bi_2S_3 unit cell, c) the crystal lattice matching between tetragonal BiOCl and orthorhombic Bi_2S_3, and d) the topotactic transformation from BiOCl disc to Bi_2S_3 disc-like network.

minimal reorganization of structure in the precursor solid, which could be the key to the formation of single-crystalline products from a single-crystalline template.[15] Namely, the lattice constant of the *a*- or *b*-axis of BiOCl was essentially unchanged during the formation of [001]-oriented Bi_2S_3 single-crystalline nanorods upon topotactic transformation from the 2D precursor template. This topotactic transformation from 2D single-crystalline discs to 2D disc-like nanorod networks represents a significant advance from the reported topotactic transformation from 1D single-crystalline nanowires to 1D single-crystalline nanostructures of another material. However, the exact mechanism responsible for the crystal-to-crystal transformation remains to be fully understood.

2.3. Effects of $BiCl_3$ and HCl Concentrations

It was found that the diameter of the Bi_2S_3 nanorods in the networks could be adjusted by changing the $BiCl_3$ concentration in the reaction solution. When the $BiCl_3$ concentration was increased from the standard concentration (i.e., 2.25 mM) to 4.5 mM, disc-like Bi_2S_3 nanorod fabrics were also obtained but the diameter of the nanorods increased from ~30 nm to ~80 nm (Fig. 7a and b). If the $BiCl_3$ concentration was decreased from the standard concentration to 1.13 mM, disc-like networks consisting of Bi_2S_3 nanorods with a diameter ~20 nm were obtained (Fig. 7c). Even thinner nanorods were formed as the $BiCl_3$ concentration was further decreased and the obtained disc-like networks apparently consisted of rather densely aligned Bi_2S_3 nanowires (Fig. 7d). This result could be rationalized by considering that a higher $BiCl_3$ concentration may result in a higher concentration of BiOCl discs in the reaction solution and a relatively slower feeding rate of the sulfide ions, leading to the formation of less Bi_2S_3 nanorod nuclei in the initial stage and hence a larger nanorod diameter in the final product.

The formation of the discs of the BiOCl precursor in the hydrolysis solution of $BiCl_3$ was essential for obtaining disc-like Bi_2S_3 nanorod networks. It was observed that an increase of the HCl concentration in the solution would prevent the precipitation of BiOCl discs, leading to the formation of Bi_2S_3 nanostructures with varied morphologies. When the HCl concentration was increased from the standard concentration (i.e., 0.07 M) to 0.15 M, only a small amount of white precipitate formed before the addition of TAA and irregularly assembled Bi_2S_3 nanostructures together with some disc-like nanorod networks were obtained finally (Fig. 8a). As the HCl concentration was increased to 1.5 M, no white precipitation was formed before the addition of TAA. Accordingly, there were no disc-like networks in the final product and only bundles of short Bi_2S_3 nanoribbons were obtained (Fig. 8b). When the HCl concentration was further

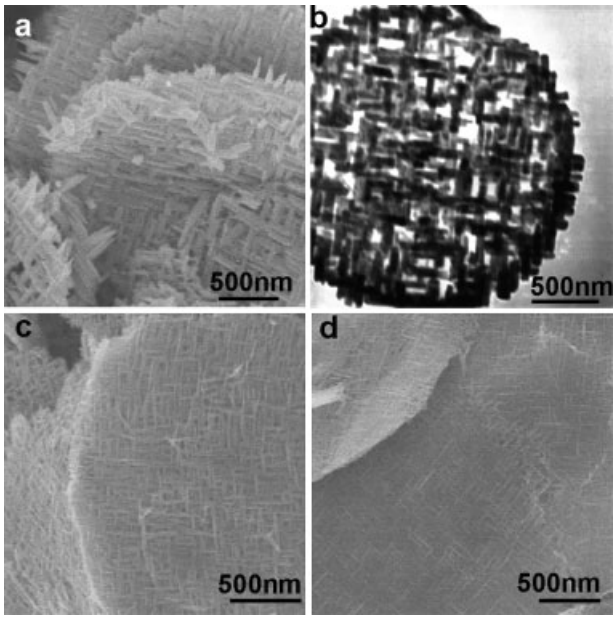

Figure 7. SEM (a, c, d) and TEM (b) images of disc-like Bi_2S_3 nanorod networks obtained at different $BiCl_3$ concentrations: a,b) 4.5 mM, c) 1.1 mM, d) 0.56 mM.

ADVANCED FUNCTIONAL MATERIALS

increased to 3 M, bundles of Bi_2S_3 nanorods about 200–300 nm in diameter and ~2 μm in length were formed (Fig. 8c and d). Figure 8e shows the TEM image of a single nanorod and the corresponding ED pattern, which exhibits diffraction spots corresponding to the $[1\bar{2}0]$ zone of the orthorhombic Bi_2S_3 with $(00L)$ spots along the rod axis direction, indicating that each nanorod is a single crystal elongated along the *c*-axis direction. The related HRTEM image (Fig. 8f) exhibits clear (210) and (001) fringes, confirming the formation of the [001]-oriented single-crystalline Bi_2S_3 nanorods.

2.4. Electrochemical Hydrogen Storage Behavior of Bi_2S_3 Nanostructures

Bismuth sulfide with a lamellar structure is expected to exhibit excellent electrochemical hydrogen storage properties; for example, it was reported that flower-like Bi_2S_3 nanostructures obtained by a biomolecule-assisted approach could electrochemically charge and discharge with the capacity of 142 mA h g^{-1} at a current density of 50 mA g^{-1} at room temperature.[20] Therefore, the electrochemical hydrogen storage behavior of the current disc-like Bi_2S_3 nanorod networks was measured at a current density of 50 mA g^{-1} at room temperature, and the charge–discharge curves displayed by the Bi_2S_3 network electrode are shown in Figure 9. It can be seen that there exist two obvious plateaus in the charging curve with the first one at ~15 mA h g^{-1} and the second one at ~65 mA h g^{-1}, indicating the presence of two different hydrogen adsorption sites in the Bi_2S_3 networks, i.e., two different electrochemical steps in the charging process.[20] It may be reasonably assumed that the hydrogen was first adsorbed into the interstitial sites/pores between Bi_2S_3 nanorods in the network structures and then entered into the interlayers of Bi_2S_3 crystals. It is noted that such a two-potential-plateau phenomenon in the charging curve was also observed in nanostructures of other materials with a lamellar structure including Ni_3S_2[31] and $Cu(OH)_2$[32] and was interpreted in a similar way. Two plateaus of the discharging potential were observed at ca. −0.30 V and −0.55 V versus Hg/HgO, and a total discharge capacity of 162 mA h g^{-1} was achieved, which is considerably higher than the capacity obtained from the flower-like Bi_2S_3 nanostructures, i.e., 142 mA h g^{-1}.[20] This could be largely attributed to the presence of more interstitial pores in the current nanorod networks. When the electrode material was replaced by the Bi_2S_3 nanorod bundles shown in Figure 8c, the discharging capacity was measured to be 109 mA h g^{-1}, much lower than that for the Bi_2S_3 nanorod networks, which could be related to the presence of much less interstitial pores in the nanorod bundles. In addition, the BET surface area of the obtained Bi_2S_3 nanorod networks was measured to be 32.3 m^2 g^{-1} and was much higher than that measured for the nanorod bundles (1.9 m^2 g^{-1}), which could also contribute to the relatively high discharging capacity for the Bi_2S_3 nanorod networks.[33,34]

Cyclic voltammograms (CVs) were also measured to further investigate the electrochemical hydrogen adsorption–desorption behaviors of the Bi_2S_3 nanostructures supported on the glassy carbon (GC) electrode (Fig. 10). In the CV of the bare GC electrode, no oxidation or reduction peak of hydrogen was observed. When the Bi_2S_3 nanorod network electrode was

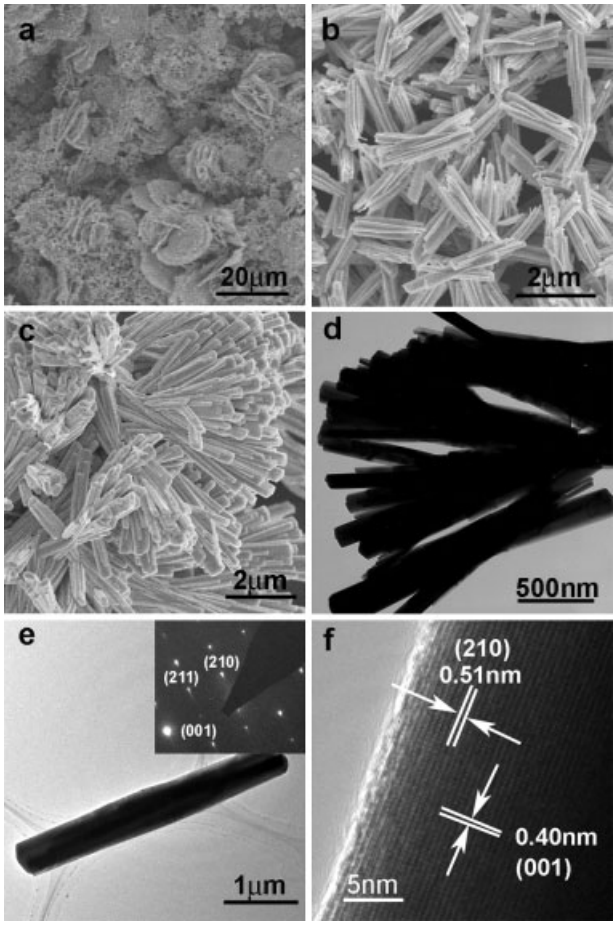

Figure 8. SEM (a–c), TEM (d, e) and HRTEM (f) images of Bi_2S_3 products obtained at different HCl concentrations: a) 0.15 M b) 1.5 M, c)–f) 3 M.

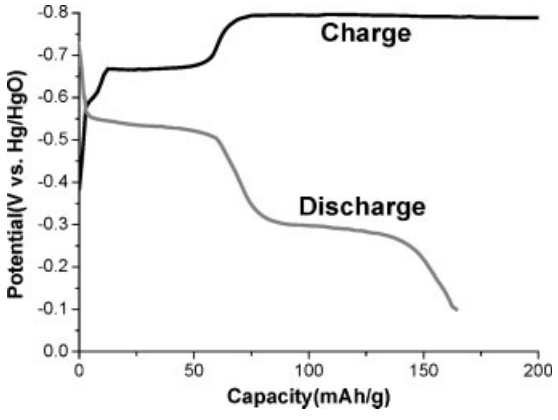

Figure 9. Charge–discharge curves of Bi_2S_3 nanorod networks. Current density: 50 mA g^{-1}.

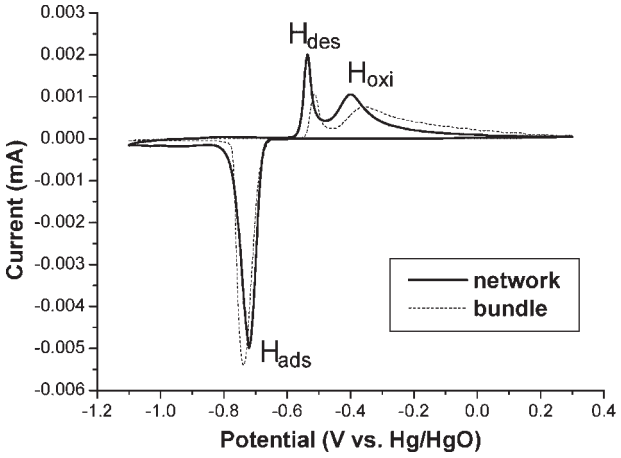

Figure 10. Cyclic voltammograms of Bi_2S_3 nanorod network and nanorod bundle electrodes. Scan rate: 50 mV s^{-1}.

used as the working electrode, one cathodic adsorption/reduction peak of hydrogen (H_{ads}) is obviously observed at ca. −0.721 V versus Hg/HgO electrode, which essentially corresponds to the two plateaus in the charging curve at −0.65 V and −0.80 V considering that the relatively faster charging rate in the CV measurement compared with the charge–discharge measurement could lead to the merging of the two hydrogen adsorption peaks. During the following anodic polarization, two current peaks appear at −0.400 V and −0.536 V. which may be attributed to the hydrogen desorption (H_{des}) and hydrogen oxidation (H_{oxi}), respectively. The occurrence of the hydrogen desorption peak prior to the hydrogen oxidation peak indicates the possible existence of the strong chemisorption of hydrogen, similar to the observations and discussion for CVs of Bi_2S_3 nanoflowers[20] and BN nanotubes.[35] These two anodic peaks could essentially correspond to the two plateaus in the discharging curve at −0.30 V and −0.55 V, respectively. For comparison purpose, the CV curves of the Bi_2S_3 nanorod bundle electrode were also measured (Fig. 10). It can be seen that one cathodic peak appears at −0.737 V, lower than that for the nanorod network electrode, and two anodic peaks appear at −0.356 V and −0.514 V, higher than those for the nanorod network electrode, respectively. This result suggest that both adsorption/reduction and desorption/oxidation of hydrogen are more difficult on the nanorod bundles. In other words, the nanorod networks are better than the nanorod bundles regarding the reversibility of hydrogen adsorption on the Bi_2S_3 nanostructures, which could contribute to the relatively high discharging capacity for the Bi_2S_3 nanorod networks in addition.

3. Conclusions

Unique, hierarchical disc-like networks consisting of a layer of crossed single-crystalline Bi_2S_3 nanorods have been synthesized via a 2D-template-engaged topotactic transformation process, which involves the formation of intermediate BiOCl single-crystalline discs and their subsequent topotactic transformation into disc-like Bi_2S_3 nanofabrics. It was revealed that these superstructures were formed by the preferential growth of [001]-oriented Bi_2S_3 nanorods on the top faces of (001)-oriented BiOCl discs along the two perpendicular [100] and [010] directions of BiOCl, which could be attributed to the close matching between the lattice constants of the *c*-axis for orthorhombic Bi_2S_3 and the *a*- or *b*-axis for tetragonal BiOCl. It was found that the formation of the discs of the BiOCl precursor in the hydrolysis solution of $BiCl_3$ was essential for obtaining disc-like Bi_2S_3 nanorod networks. The diameter of the Bi_2S_3 nanorods involved in the networks could be adjusted by changing the bismuth ion concentration in the reaction solution; moreover, an increase of the HCl concentration would prevent the formation of precursor BiOCl discs, leading to the formation of Bi_2S_3 nanostructures with varied morphologies, such as bundles of nanoribbons/nanorods. The obtained disc-like Bi_2S_3 nanorod networks could electrochemically charge and discharge with a capacity of 162 mA h g^{-1} at room temperature, indicating their potential applications in hydrogen storage, high-energy batteries, and catalytic fields. Furthermore, the unusual architecture of disc-like networks made of crossed semiconductor nanorods may provide an interesting modal system for fundamental studies. This work demonstrates for the first time that a topotactic transformation process can be employed for the topotactic transformation into 2D networks consisting of single-crystalline nanorods from a 2D single-crystalline template. This approach is potentially extendable to the fabrication of 2D networks made of 1D single-crystalline nanostructures with desirable properties and could open new avenues for the bottom-up fabrication of nanodevices assembled from 1D nanostructures.

4. Experimental

Materials: Bismuth chloride ($BiCl_3$, A.R) and thioacetamide (TAA, A.R) were purchased from Sinopharm Chemical Reagent Co. Ltd and used as received. Hydrochloric acid was supplied by Beijing Chemical Regent Co. The water used was deionized.

Synthesis of Bi_2S_3 Nanostructures: In a standard synthesis of Bi_2S_3 nanorod networks, 50 μL of $BiCl_3$ (0.1 M) and HCl (3 M) solution was first added to 2 mL water at room temperature, leading to the formation of a white precipitate. Then, 200 μL of TAA solution (0.5 M) was added and the mixture was incubated at 60 °C for 60 hours, resulting in the formation of a black precipitate. The black precipitate was collected and washed three times with distilled water. Moreover, the $BiCl_3$ concentration in the initial 50 μL solution was systematically varied to investigate the effect of the $BiCl_3$ concentration and the 2 mL water was replaced by 2 mL HCl solution with different concentrations to investigate the effect of the HCl concentration.

Characterization: The obtained products were characterized by SEM (Hitachi, S-4800, 5 kV), TEM (JEOL JEM-200CX, 160 kV), HRTEM (FEI Tecnai F30, 300 kV), XRD (Rigaku Dmax-2000 with Cu Kα radiation). Nitrogen adsorption–desorption measurements were performed using Micromeritics ASAP 2010.

Electrochemical Measurements: Charge–discharge measurements were carried out following the reported method [36] with minor modification by using the Land battery system (CT2001A) at room temperature ((25 ± 2) °C). Briefly, the electrode was fabricated by

ADVANCED FUNCTIONAL MATERIALS

directly pressing the synthesized Bi_2S_3 powders on a sheet of nickel foam at 50 MPa. All of the measurements were performed in a three-electrode cell in 5 M KOH under normal atmosphere. The Bi_2S_3 nanostructures were used as the working electrode, $Ni(OH)_2$/NiOOH as the counter electrode, and Hg/HgO as the reference electrode. The Bi_2S_3 nanostructure electrode was charged for 4 h at a current density after a 2 s rest.

Cyclic voltammograms measurements were performed on a CHI 660A electrochemical workstation (Shanghai CH Instruments, China) with a conventional three-electrode cell at room temperature ($(25 \pm 2)\,^{\circ}C$). The working electrode was a glassy carbon (GC) electrode modified with the Bi_2S_3 nanostructures. For the preparation of Bi_2S_3-modified electrodes, the GC electrode with a diameter of 4 mm was first polished with 0.05 μm alumina slurry and then washed ultrasonically in triply distilled water and ethanol for a few minutes. The prepared Bi_2S_3 nanostructures were dispersed in water to obtain a uniform suspension of $22.5\,mg \cdot mL^{-1}$ by sonication. Then, the GC electrodes were coated by casting 10 μL of the above Bi_2S_3 suspension and dried under an infrared lamp. Finally, 1 wt% Nafion solution in alcohol was cast on the surface of the sample and dried naturally in the air.

Received: December 14, 2007
Revised: January 17, 2008

[1] a) Y. Xia, P. Yang, Y. Sun, Y. Wu, B. Mayers, B. Gates, Y. Yin, F. Kim, H. Yan, *Adv. Mater.* **2003**, *15*, 353. b) C. Thelander, P. Agarwal, S. Brongersma, J. Eymery, L. F. Feiner, A. Forchel, M. Scheffler, W. Riess, B. J. Ohlsson, U. Gösele,1 L. Samuelson, *Mater. Today* **2006**, *9*, 28. c) P. J. Pauzauskie, P. Yang, *Mater. Today* **2006**, *9*, 36. d) F. Patolsky, B. P. Timko, G. G. Zheng, C. M. Lieber, *MRS Bull.* **2007**, *32*, 142.

[2] a) L. Manna, D. J. Milliron, A. Meidel, E. C. Scher, A. P. Alivisatos, *Nat. Mater.* **2003**, *2*, 382. b) P. Yang, *MRS Bull.* **2005**, *30*, 85. c) A. J. Mieszawska, R. Jalilian, G. U. Sumanasekera, F. P. Zamborini, *Small* **2007**, *3*, 722. d) C. M. Lieber, Z. L. Wang, *MRS Bull.* **2007**, *32*, 99.

[3] a) M. Li, H. Schnablegger, S. Mann, *Nature* **1999**, *402*, 393. b) F. Kim, S. Kwan, J. Akana, P. Yang, *J. Am. Chem. Soc.* **2001**, *123*, 4360. c) D. Whang, S. Jin, Y. Wu, C. M. Lieber, *Nano Lett.* **2003**, *3*, 1255. d) K. K. Caswell, J. N. Wilson, U. H. F. Bunz, C. J. Murphy, *J. Am. Chem. Soc.* **2003**, *125*, 13914. e) N. R. Jana, *Angew. Chem. Int. Ed.* **2004**, *43*, 1536.

[4] a) H. J. Fan, P. Werner, M. Zacharias, *Small* **2006**, *2*, 700. b) E. J. W. Crossland, S. Ludwigs, M. A. Hillmyer, U. Steiner, *Soft Matter* **2007**, *3*, 94.

[5] a) J. Y. Lao, J. G. Wen, Z. F. Ren, *Nano Lett.* **2002**, *2*, 1287. b) H. Yan, R. He, J. Johnson, M. Law, R. J. Saykally, P. Yang, *J. Am. Chen. Soc.* **2003**, *125*, 4728. c) P. X. Gao, Z. L. Wang, *Appl. Phys. Lett.* **2004**, *84*, 2883. d) M. J. Bierman, Y. K. A. Lau, S. Jin, *Nano Lett.* **2007**, *7*, 2907.

[6] a) Z. A. Peng, X. Peng, *J. Am. Chen. Soc.* **2002**, *124*, 3343. b) Y. Jun, Y. Jing, J. Cheon, *J. Am. Chem. Soc.* **2002**, *124*, 615. c) S. Chen, Z. L. Wang, J. Ballato, S. H. Foulger, D. L. Carroll, *J. Am. Chem. Soc.* **2003**, *125*, 16186.

[7] a) L. Qi, H. Cölfen, M. Antonietti, M. Li, J. D. Hopwood, A. J. Ashley, S. Mann, *Chem. Eur. J.* **2001**, *7*, 3526. b) S. H. Yu, M. Antonietti, H. Cölfen, J. Hartmann, *Nano Lett.* **2003**, *3*, 379.

[8] a) H. Shi, L. Qi, J. Ma, H. Cheng, *J. Am. Chem. Soc.* **2003**, *125*, 3450. b) H. Shi, L. Qi, J. Ma, N. Wu, *Adv. Funct. Mater.* **2005**, *15*, 442.

[9] Q. Lu, F. Gao, S. Komarneni, *J. Am. Chem. Soc.* **2004**, *126*, 54.

[10] H. Uchiyama, H. Imai, *Cryst. Growth Des.* **2007**, *7*, 841.

[11] a) H. Dai, E. W. Wong, Y. Z. Lu, S. Fan, C. M. Lieber, *Nature* **1995**, *375*, 769. b) C. Tang, S. Fan, M. L. de la Chapelle, H. Dang, P. Li, *Adv. Mater.* **2000**, *12*, 1346.

[12] Y. Wu, B. Messer, P. Yang, *Adv. Mater.* **2001**, *13*, 1487.

[13] J. Goldberger, R. R. He, Y. F. Zhang, S. Lee, H. Q. Yan, H.-J. Choi, P. D. Yang, *Nature* **2003**, *422*, 599.

[14] J. H. Song, Y. Wu, B. Messer, H. Kind, P. Yang, *J. Am. Chem. Soc.* **2001**, *123*, 10397.

[15] a) B. Gates, Y. Wu, Y. Yin, P. Yang, Y. Xia, *J. Am. Chem. Soc.* **2001**, *123*, 11500. b) B. Gates, B. Mayers, Y. Wu, Y. Sun, B. Cattle, P. Yang, Y. Xia, *Adv. Funct. Mater.* **2002**, *12*, 679. c) U. Jeong, P. H. C. Camargo, Y. H. Lee, Y. Xia, *J. Mater. Chem.* **2006**, *16*, 3893.

[16] D. H. Son, S. M. Hughes, Y. Yin, A. P. Alivisatos, *Science* **2004**, *306*, 1009.

[17] R. Suarez, P. K. Nair, P. V. Kamat, *Langmuir* **1998**, *14*, 3236.

[18] S.-C. Liufu, L.-D. Chen, Q. Yao, C.-F. Wang, *Appl. Phys. Lett.* **2007**, *90*, 112106.

[19] O. Rabin, J. M. Perez, J. Grimm, G. Wojtkiewicz, R. Weissleder, *Nat. Mater.* **2006**, *5*, 117.

[20] B. Zhang, X. Ye, W. Hou, Y. Zhao, Y. Xie, *J. Phys. Chem. B* **2006**, *110*, 8978.

[21] a) Z. Liu, S. Peng, Q. Xie, Z. Hu, Y. Yang, S. Zhang, Y. Qian, *Adv. Mater.* **2003**, *15*, 936. b) F. Wei, J. Zhang, L. Wang, Z.-K. Zhang, *Cryst. Growth Des.* **2006**, *6*, 1942. c) Y. Zhao, X. Zhu, Y. Huang, S. Wang, J. Yang, Y. Xie, *J. Phys. Chem. C.* **2007**, *111*, 12145. d) J. Ota, S. K. Srivastava, *J. Phys. Chem. C.* **2007**, *111*, 12260. e) Q. Han, J. Chen, X. Yang, L. Lu, X. Wang, *J. Phys. Chem. C.* **2007**, *111*, 14072. f) W. Lou, M. Chen, X. Wang, W. Liu, *Chem. Mater.* **2007**, *19*, 872.

[22] R. Chen, M. H. So, C.-M. Che, H. Sun, *J. Mater. Chem.* **2005**, *15*, 4540.

[23] B. Sigman, Jr., B. A. Korgel, *Chem. Mater.* **2005**, *17*, 1655.

[24] H. Bao, X. Cui, C. M. Li, Y. Gan, J. Zhang, J. Guo, *J. Phys. Chem. C.* **2007**, *111*, 12279.

[25] J. Xu, N. Petkov, X. Wu, D. Iacopino, A. J. Quinn, G. Redmond, T. Bein, M. A. Morris, J. D. Holmes, *ChemPhysChem* **2007**, *8*, 235.

[26] S.-C. Liufu, L.-D. Chen, Q. Wang, Q. Yao, *Cryst. Growth Des.* **2007**, *7*, 639.

[27] C. Jiang, S.-H. Yu, W.-T. Yao, H. Ge, G.-Z. Zhang, *Chem. Mater.* **2005**, *17*, 6094.

[28] X. Zhou, S. Chen, D. Zhang, X. Guo, W. Ding, Y. Chen, *Langmuir* **2006**, *22*, 1383.

[29] J. Tang, A. P. Alivisatos, *Nano Lett.* **2006**, *6*, 2701.

[30] R. Malakooti, L. Cademartiri, Y. Akçakir, S. Petrov, A. Migliori, G. A. Ozin, *Adv. Mater.* **2006**, *18*, 2189.

[31] B. Zhang, X. Ye, W. Dai, W. Hou, Y. Xie, *Chem. Eur. J.* **2006**, *12*, 2337.

[32] P. Gao, M. Zhang, Z. Niu, Q. Xiao, *Chem. Commun.* **2007**, 5197.

[33] J. Chen, N. Kuriyama, H. Yuan, H. T. Takeshita, T. Sakai, *J. Am. Chem. Soc.* **2001**, *123*, 11813.

[34] B. Fang, H. Zhou, I. Honma, *J. Phys. Chem. B* **2006**, *110*, 4875.

[35] X. Chen, X. P. Gao, H. Zhang, Z. Zhou, W. K. Hu, G. L. Pan, H. Y. Zhu, T. Y. Yan, D. Y. Song, *J. Phys. Chem. B* **2005**, *109*, 11525.

[36] G. P. Dai, C. Liu, M. Liu, M. Z. Wang, H. M. Cheng, *Nano Lett.* **2002**, *2*, 503.

